Research Article

Chenming Zhang, Yihua Cui*, Shiping Lin, and Jianwei Guo

Preparation and applications of hydrophilic quaternary ammonium salt type polymeric antistatic agents

https://doi.org/10.1515/epoly-2022-0035
received February 19, 2022; accepted March 18, 2022

Abstract: A novel ammonium salt type polymeric antistatic agent (PDSH) was synthesized from methacrylatoethyl trimethyl ammonium chloride, styrene, and 2-hydroxyethyl methacrylate via radical polymerization. Antistatic poly (acrylonitrile-*co*-butadiene-*co*-styrene) (ABS)/PDSH composites were prepared by blending PDSH with ABS resin. The results showed that the surface resistivity of ABS/PDSH composites with PDSH addition decreased significantly. The surface resistivity of ABS/PDSH composites containing 20 wt% PDSH was around 10^9–10^{10} Ω, which was about 10^6 times lower than that of neat ABS. At the same time, ABS/PDSH composites had good thermal stability and hydrophilicity. The PDSH was more uniformly dispersed within the ABS resin and had less influence on the mechanical properties of the composites. With the demonstrated properties, the prepared copolymer PDSH can serve as a well-integrated antistatic agent and display potential for the antistatic treatment of ABS.

Keywords: antistatic, copolymer, ABS composites, surface resistivity

1 Introduction

Poly(acrylonitrile-*co*-butadiene-*co*-styrene) (ABS) is a thermoplastic engineering plastic with excellent chemical resistance, mechanical properties, and processing performance, which has a wide range of applications in the manufacturing industry (1–3). However, ABS has low electrical conductivity and obvious hydrophobicity (4), and the surface resistivity is as high as 10^{14}–10^{16} Ω. The result is that ABS is prone to the accumulation of electrical charges on the surface. In severe cases, static electricity may cause fires and explosions (5–7), which limits the application of ABS in the field of communications (8), new energy vehicles (9), and aerospace (10). Therefore, it is of great significance to develop antistatic ABS with excellent comprehensive properties.

Researchers have made many efforts to improve the antistatic properties of polymers. Conventional antistatic agents are usually composed of amphiphilic surfactants (11). Affected by friction or washing, the antistatic agents on the surface are easy to disappear and cannot achieve the permanent antistatic effect (10,12). The addition of conductive fillers, such as carbon black (13), carbon nanotubes (14), graphene (15), metal oxides (8), and conductive polymers (16), to the matrix resin can effectively reduce the surface resistivity of the polymers. However, for these conductive fillers, mobility and poor compatibility with the matrix resin have become obstacles in their application (17,18).

In recent years, polymer antistatic agents have attracted more and more concerns, which exhibit excellent antistatic properties, long-lasting effects, and good compatibility with the matrix resin (19–22). In particular, quaternary ammonium salt-based copolymers are currently of considerable academic and industrial interest, owing to their enhanced charge density and polarity, which is beneficial to the antistatic properties and hydrophilic of the antistatic agents (23,24). Although the quaternary ammonium salt-based copolymer antistatic agents have good antistatic properties and hygroscopic properties, the enhancement of polarity reduces the compatibility of the copolymer with the matrix resin and is prone to agglomeration, which has a significant impact on the physical and morphological properties of the material. Therefore, a low-polarity monomer needs to be introduced to improve the compatibility of the copolymer with the matrix resin.

* **Corresponding author: Yihua Cui,** School of Chemical Engineering and Light Industry, Guangdong University of Technology, Guangzhou, China, e-mail: cuiyihuagdut@163.com
Chenming Zhang, Jianwei Guo: School of Chemical Engineering and Light Industry, Guangdong University of Technology, Guangzhou, China
Shiping Lin: Pengrun Die Casting Material Technology Co., Dongguan, China

Open Access. © 2022 Chenming Zhang *et al.*, published by De Gruyter. This work is licensed under the Creative Commons Attribution 4.0 International License.

In this article, a novel random copolymer antistatic agent (PDSH) was synthesized by free-radical solution polymerization using methacrylatoethyl trimethyl ammonium chloride (DMC), styrene (ST), and 2-hydroxyethyl methacrylate (HEMA) as raw materials. DMC was used as the main antistatic component. HEMA was beneficial to promote water absorption and the cationic dissociation of quaternary ammonium salt. Low polar component ST helped to improve the compatibility between the copolymers and the matrix resin. ABS/PDSH composites were prepared by blending PDSH with ABS resin in a two-roll mill, and their surface resistivity, thermal properties, hydrophilicity, mechanical properties, and morphology were characterized.

2 Materials and methods

2.1 Materials

DMC (75%, 600 ppm MEHQ), ST (99%, 10-15 ppm TBC), and neutral alumina were obtained from Maclin Biochemical Technology Co., Ltd (Shanghai, China). HEMA (99%, 200 ppm MEHQ) and 2,2-azobis (isobutyronitrile) (AIBN, 99%) were purchased from Aladdin Biochemical Technology Co., Ltd (Shanghai, China). Anhydrous ethanol (AR) and toluene (AR) were purchased from Guangzhou Chemical Reagent Factory. ABS resin was purchased from Taiwan's Chi Mei Industrial Co., Ltd. Antioxygen 1010 was purchased from BASF China Co., Ltd. DMC and HEMA were purified first by passing through a column filled with neutral alumina before use. All other reagents were used without any further treatment.

2.2 Synthesis of PDSH copolymers

PDSH copolymers were synthesized by free-radical solution polymerization in absolute ethanol using DMC, ST, and HEMA as raw materials. The reaction was carried out in a three-necked flask equipped with a stirring device, condensation reflux device, and thermometer. In the nitrogen atmosphere, absolute ethanol and all reaction monomers (DMC, ST, and HEMA) were added to a three-necked flask. The molar ratio of the various monomers (DMC, ST, and HEMA) was 10:9:1, 10:7:3, 10:5:5, 10:3:7, and 10:1:9, respectively. After stirring at 200 rpm for 10 min, a certain amount of initiator AIBN was added. The temperature was slowly raised to 75°C, and the reaction was carried out for 6 h. After the reaction, about 80% ethanol was evaporated by a rotary evaporator. The reaction products were precipitated with toluene and dried under a vacuum at 80°C for 24 h. The synthetic route of PDSH is shown in Scheme 1.

2.3 Preparation of ABS/PDSH composites

Before blending, PDSH, ABS resin, and antioxygen were vacuum dried at 80°C for 12 h. Certain amounts of PDSH, antioxidant, and ABS resin were mixed at 185°C for 10 min with a two-roll mill at a speed of 50 rpm. The mixed ABS composite material was molded at 185°C with a vulcanizer.

2.4 Characterization

Infrared spectra were recorded on an iS50R infrared spectrometer (THEMOR-FILSHER, USA) in the range of 4,000–400 cm^{-1}. The NMR test was carried out on the AVANCE III HD 400 spectrometer (Bruker, Switzerland), and DMSO-d_6 was selected as the solvent. Matrix-assisted laser desorption ionization time-of-flight mass spectra (MALDI-TOF MS) were acquired on a Bruker Ultraflextreme TOF/TOF mass spectrometer (Bruker, Germany). The samples were dispersed in ethanol, and α-cyano-4-hydroxycinnamic acid was chosen as the matrix.

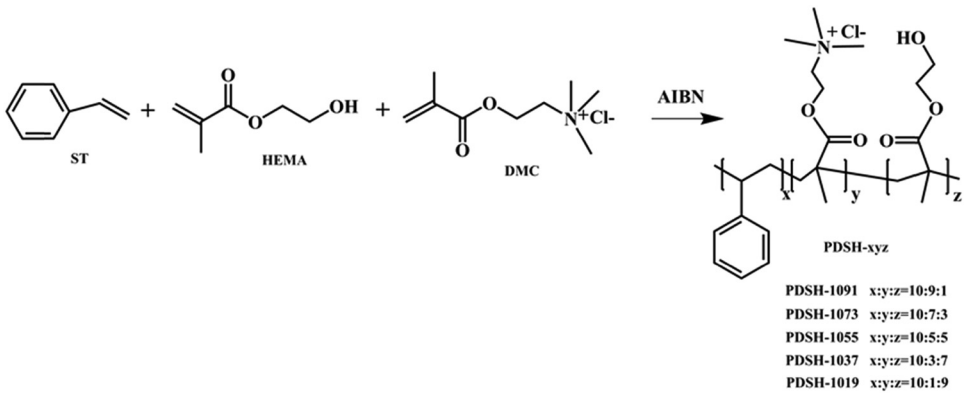

Scheme 1: Schematic diagram of PDSH synthesis.

The thermal stability of PDSH and ABS/PDSH was investigated by TGA testing on a STA449F5 (NETZSCH, Germany) thermogravimetric analyzer. The samples were heated at a rate of 10°C·min^{-1} under an N_2 atmosphere, from 30°C to 600°C.

DSC3 analyzer (Mettler-Toledo, Switzerland) was used in differential scanning calorimetry (DSC). Samples were heated in the first heating run (25–200°C), cooling (200–25°C), and second heating (25–200°C), with a rate of 10°C·min^{-1}. The glass transition (T_g) temperatures were measured during the second heating process. The samples were tested under 50 mL·min^{-1} of nitrogen flow.

The surface resistivity of neat ABS and ABS/PDSH composites was measured according to GB/T 31838.3-2019 using a ZC36 megohmmeter (Shanghai Precision Co., Ltd., China) with a set voltage of 500 V. The samples were placed at 23°C and 50% relative humidity for 24 h before analysis.

The static contact angles of the composites were measured at room temperature according to the sessile drop method using a video optical contact angle meter of OCA100 (Dataphysics, Germany). Place a drop of distilled water (2 µL) at a rate of 0.5 µL·s^{-1} using a microsyringe. Images of the droplets were recorded 10 s after the droplets were initially placed on the composite surface.

The section morphology of neat ABS and ABS/PDSH composites was observed by TESCAN CLARA field emission scanning electron microscope (SEM, TESCAN, Czechoslovakia) at 10 kV accelerating voltage. The SEM was connected with energy-dispersive X-ray spectroscopy (EDS/Xplore 30) to characterize the elemental composition of the ABS/PDSH composite section, and the elemental distribution map of the section was obtained. Before the test, the samples were brittle in liquid nitrogen, and the surface of the samples was coated with gold.

The notch impact strength was tested with an XBL-5.5D digital display pendulum impact tester (Guangzhou Puyang Instrument Co., Ltd., China) according to GB/T 1043.1-2008. Tensile strength was tested with an Inspekt Table Blue 5 kN universal electronic testing machine (Hegewald & Peschke, Germany) according to GB/T 1040.1-2018. The mechanical properties were tested at 23°C and 50% relative humidity.

3 Results and discussion

3.1 Structural characterization

Figure 1 shows the FTIR spectra of DMC, ST, HEMA, and PDSH-1055. It can be seen that PDSH has a C=O absorption peak at 1,725 cm^{-1}, and a stretch vibration peak of C–O–C at 1,145 cm^{-1}, so the presence of the ester group can be determined. The bending vibration absorption peak of methylene in the cationic group $-CH_2-N^+$ appears at 1,454 cm^{-1}, the characteristic absorption peak of methyl in $-CH_2-N^+(CH_3)_3$ appears at 952 cm^{-1}, and the stretching vibration peak of $-CH_3$ appears at 1,388 cm^{-1}, which can prove the presence of DMC unit in the copolymer. The benzene ring skeleton vibration peaks at 1,490 and 1,601 cm^{-1}, and a powerful absorption peak at 701 cm^{-1}, which was generated by the –CH bending vibration of monosubstituted benzene, indicated that the ST unit was successfully introduced into the PDSH. In Figure 1, each monomer has a C=C absorption peak at 1,640 cm^{-1}, and the characteristic peak at 1,640 cm^{-1} in the FTIR spectrum of PDSH disappears, indicating that the three monomers react entirely.

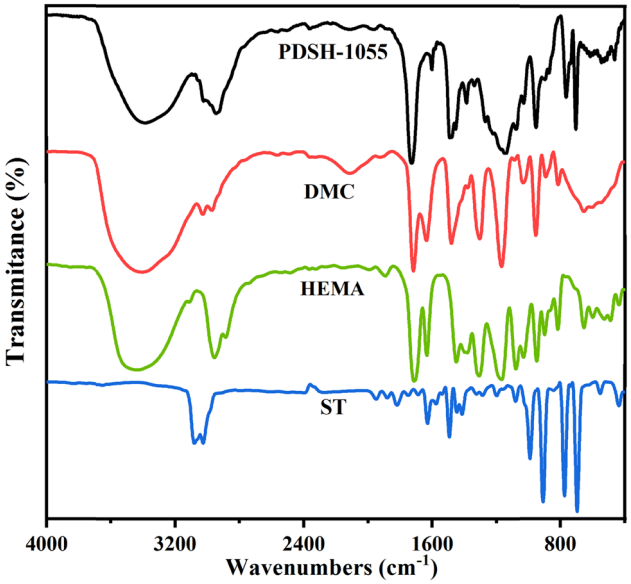

Figure 1: FTIR spectra of PDSH-1055, DMC, HEMA, and ST.

Figure 2 shows the ^{1}H NMR spectrum of PDSH-1055. It can be seen from the spectrum that the –OH characteristic resonance appears at $\delta = 4.9$, and the characteristic resonance of $-CH_2$ on the main chain in the HEMA unit appears at $\delta = 2.3$. From this, the presence of HEMA units in the copolymer can be demonstrated. On the other hand, the stretching vibration peak of the benzene ring skeleton appears at $\delta = 6.5–8.5$, and the characteristic resonance doublet of $-CH_3$ bound to the N^+ ion of the cationic unit appears at $\delta = 3.11–3.15$. It was demonstrated that DMC and ST units were incorporated into the copolymer, which would further confirm the results obtained by the IR spectra. MALDI-TOF was used to measure the molecular weight of PDSH, and the results are shown in Figure 3. The results showed that the molecular

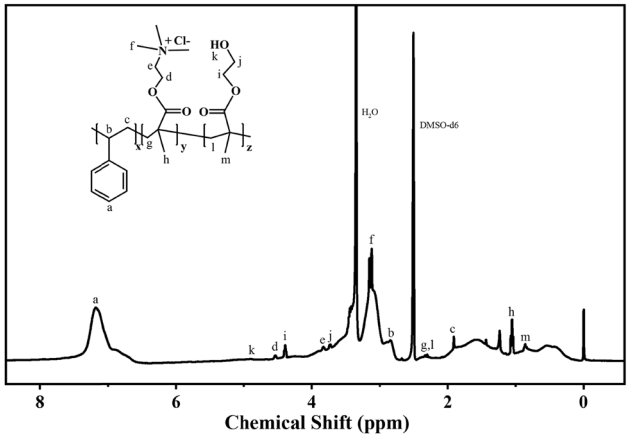

Figure 2: ^{1}H NMR spectra of PDSH-1055 in DMSO-d_6.

weights of PDSH synthesized with different molar ratios of monomers were all in the range of 280,000–390,000 Da. The above information indicates that the PDSH copolymer was successfully synthesized.

3.2 Thermal properties

The thermal stability and initial decomposition (5% weight loss) temperature of PDSH and ABS/PDSH composites were investigated by TGA. The TGA curves of antistatic copolymers with different monomer ratios are shown in Figure 4. PDSH undergoes two weight losses during the temperature rise process. The first weight loss of around 220°C could be attributed to the thermal decomposition of the quaternary ammonium salt component (25). The weight loss was most obvious in the second stage above 350°C, and the pyrolysis process was mainly the decomposition of the PDSH main chain (20). The thermal decomposition

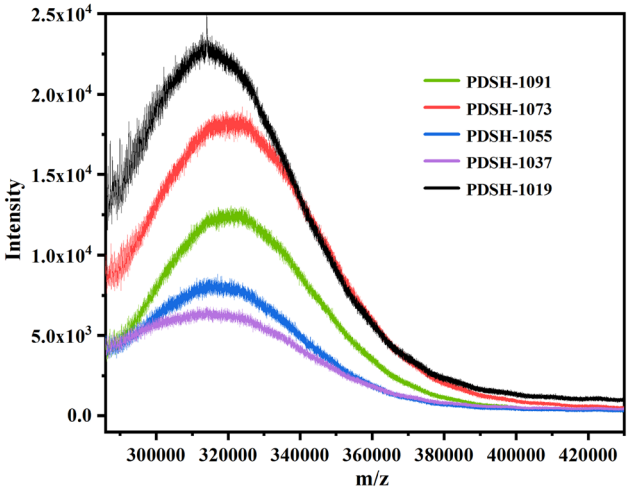

Figure 3: MALDI-TOF spectra of PDSH.

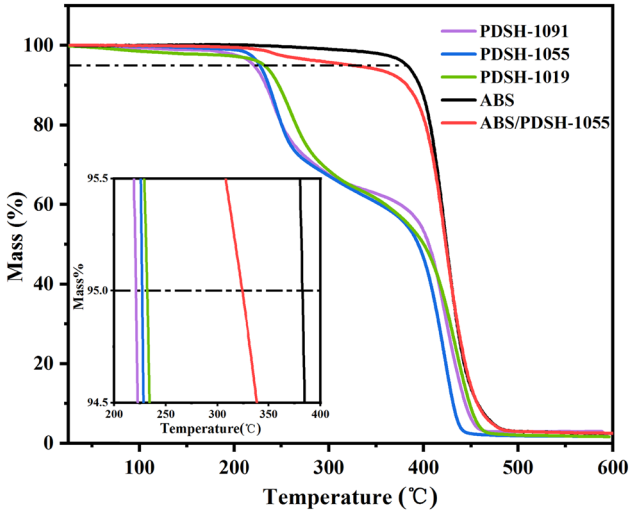

Figure 4: TGA curves of PDSH, ABS, and ABS/PDSH composites.

ended when the temperature exceeded 460°C. The initial decomposition temperature of PDSH-1091 was 220.9°C, which was nearly 12°C lower than that of PDSH-1019. The increase in the content of the HEMA component raises the initial decomposition temperature of the PDSH copolymer. The TGA curves for neat ABS and ABS/PDSH-1055 with 10 wt% PDSH are also given in Figure 4. The starting decomposition temperature of ABS/PDSH-1055 was 343°C, while that of ABS was 382°C. The main reason for the decrease in the starting decomposition temperature of the composites after adding PDSH is the decomposition of the quaternary ammonium salt component in PDSH, which corresponds to the weight loss of the first segment in the TGA of PDSH. In general, both PDSH and ABS/PDSH are thermally stable below 220°C and do not thermally decompose during the blending and molding stages.

To investigate the thermal transition temperature of the copolymers, DSC analysis was performed on PDSH, neat ABS, and ABS/PDSH composites with 20 wt% antistatic agents. It can be found from Figure 5 that only one T_g appears in the DSC curve of PDSH, which indicates that PDSH was an amorphous copolymer. The T_g of PDSH increased from 151.5°C to 158.9°C with the increase of ST component content. In the second heating process test, both neat ABS and ABS/PDSH composites showed T_g around 108°C. The addition of PDSH had less effect on the thermal properties of ABS resin.

3.3 Antistatic properties of the ABS/PDSH composites

Figure 6 demonstrates the effect of PDSH addition on the surface resistivity of ABS/PDSH composites at 23°C and

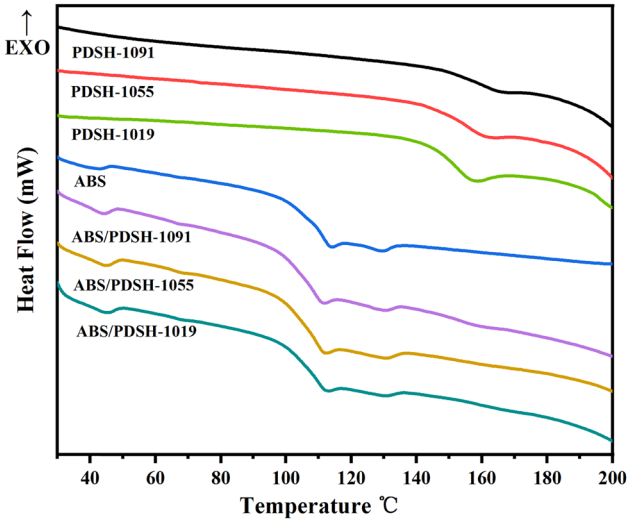

Figure 5: DSC thermograms of PDSH, ABS, and ABS/PDSH composites.

50% relative humidity. It can be seen from Figure 6 that the surface resistivity of ABS/PDSH composites decreases significantly with the increase of PDSH addition. With the addition of PDSH of less than 15 wt%, the surface resistivity of ABS/PDSH composites decreased rapidly from 10^{15} to 10^{9}–10^{10} Ω with the increase of PDSH content. When the addition of PDSH exceeded 15 wt%, the surface resistivity decreased slightly. With the increase in the PDSH above 20 wt%, the surface resistivity of the composites was also maintained at 10^{9}–10^{10} Ω. It shows that the

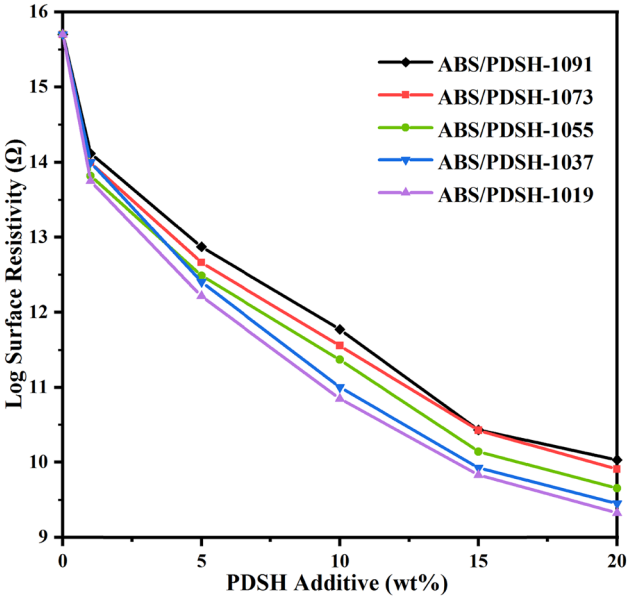

Figure 6: Surface resistivity changes of ABS/PDSH composites as a function of the antistatic agent content (wt%).

percolation threshold of PDSH is close to 15 wt%. Larger gaps of conductive elements in the polymer matrix lead to higher energy barriers with a less antistatic agent added. When the added amount of the antistatic agent reaches the percolation threshold, the distance between the antistatic copolymer in the ABS resin is shortened to form a continuous conductive network. After the threshold value is reached, the surface resistivity of the composite material will only decrease slightly after adding the antistatic agent because the conductive network has been formed (22). Another significant result in Figure 6 is that the surface resistivity of the composites decreases with the increase of the HEMA component content at the same addition. For example, when the PDSH content was 10 wt%, the surface resistivities of ABS/PDSH-1019 and ABS/PDSH-1091 were 7.05×10^{10} and 5.9×10^{11} Ω, respectively. This result is due to the fact that the –OH in the HEMA component contains sp_3-hybridized O atoms that can form coordination effects with the N atoms in DMC, which can effectively dissociate DMC to form more quaternary ammonium cations to improve ionic conductivity (21). On the other hand, the increase in the content of HEMA components leads to an increase in the hydrophilic region in the composite. The quaternary ammonium salt component and –OH can adsorb moisture from the air, and the water molecules are involved in forming the surface conductive network to reduce the surface resistivity (5,26,27).

The current copolymer antistatic agent research was widespread, but the application of quaternary ammonium salt-based copolymer antistatic agents was less reported. It was reported that for polyether-type antistatic agents, the surface resistivity of ABS could reach 10^{11} Ω at an addition level of 20 wt% (20). In another work, 12 wt% polyether block amide was used to achieve 10^{10} Ω surface resistivity for ABS matrix resin (28). In this work, the surface resistivity of the composite has been reduced to 6.78×10^{9} Ω when the content of PDSH-1019 reaches 15 wt%. Compared with the neat ABS resin, the surface resistivity of the ABS composites was reduced by about 10^{6} times, which could meet the antistatic needs of ABS in most cases.

3.4 Hydrophilic properties

Figure 7 shows the water contact angle results for the ABS/PDSH blended system as a means of examining the hydrophilicity of the ABS/PDSH blended system. The contact angle (θ) of neat ABS was 97°, and the contact angle of the composites decreased gradually after the

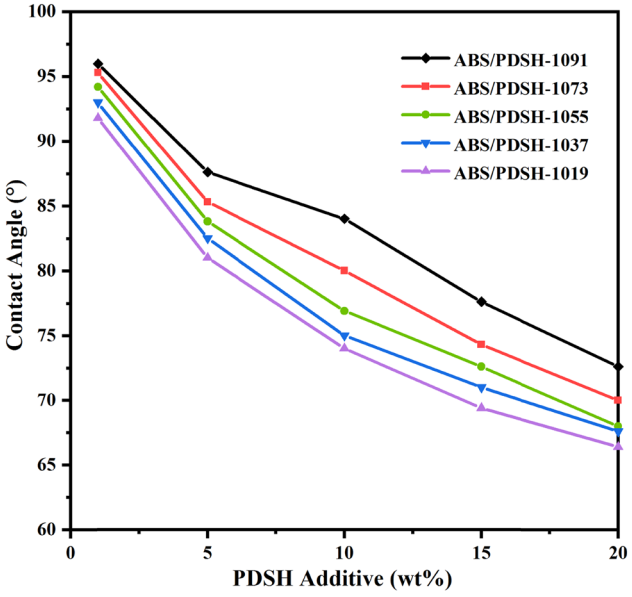

Figure 7: Contact angle values of ABS/PDSH composites as a function of the antistatic agent content (wt%).

addition of PDSH. When the content of the copolymer was 20 wt%, the θ of the ABS/PDSH-1019 composite decreased to 66°. In addition, the θ values of the composites showed a decreasing trend as the content of the HEMA component increased. When PDSH-1019 was used as an antistatic agent, the θ value of the composite decreased rapidly, reaching 74° when the content of the copolymer was 10 wt%. These results are due to the presence of the more polar and hydrophilic quaternary ammonium salts and –OH in PDSH, resulting in a better hydrophilic ABS/PDSH composite after blending. The hydrophilicity of the composite is further enhanced when the content of the HEMA component containing –OH is increased (23,29).

3.5 Morphology

Figure 8a–f shows the SEM images of neat ABS and ABS/PDSH-1091 with 20 wt% PDSH at different magnifications, respectively. In Figure 8a and d, the cross-sections

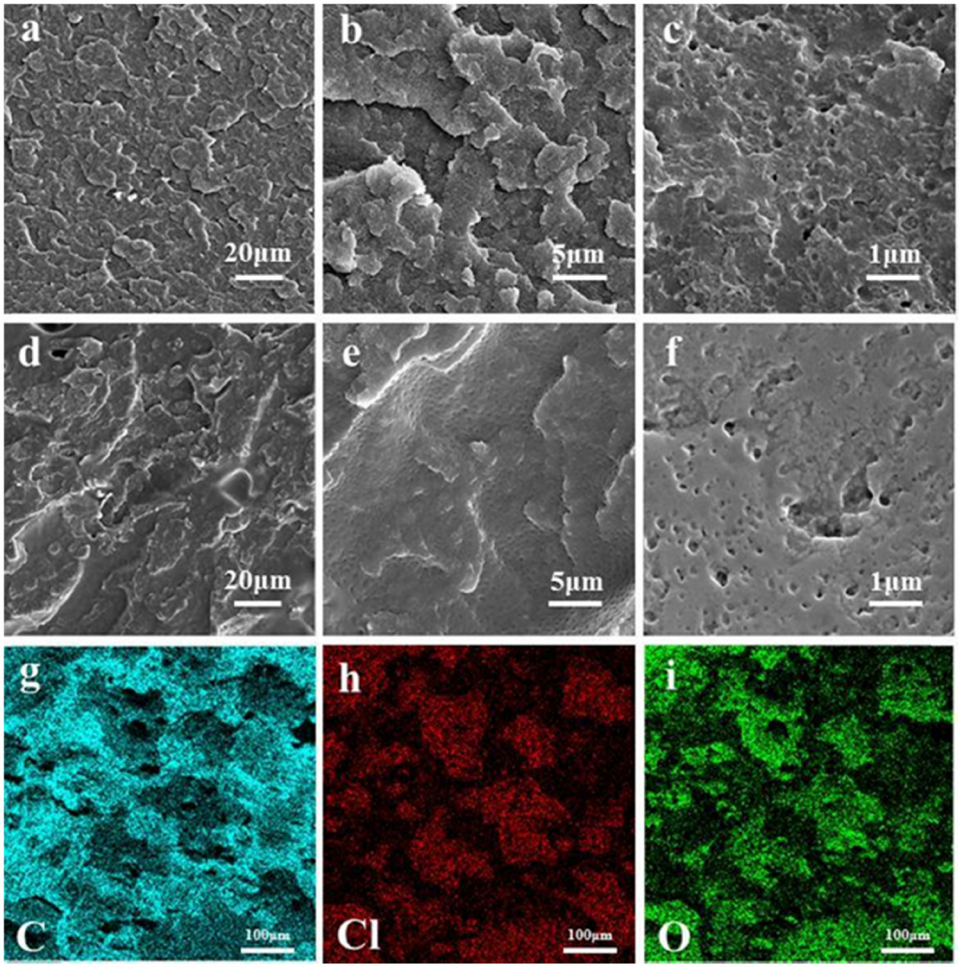

Figure 8: SEM photos of (a–c) neat ABS, (d–f) ABS with 20 wt% PDSH-1091. EDS elemental maps of (g–i) ABS with 20 wt% PDSH-1091.

of ABS and ABS/PDSH-1091 composites were layered structures. The composites had a smoother cross-section compared to ABS resin, resulting from the blending of PDSH with ABS resin. From Figure 8b and e, it can be seen that the ABS/PDSH-1091 composite showed a dense concentration of holes compared to the neat ABS, which were evenly distributed throughout the composites. At higher magnification, Figure 8c shows a small number of holes in the neat ABS. Figure 8f shows that after the addition of PDSH in addition to the cavities, there was a uniform distribution of small solid holes, which were formed by the PDSH antistatic agents dispersed uniformly in the matrix resin. The addition of the ST component enhances the compatibility of the antistatic agent with the ABS resin so that the PDSH can be evenly dispersed in the ABS resin. Antistatic agents are evenly distributed in the matrix resin to form a conductive network. Electrons can transit through the conductive network and dissipate quickly to reduce the surface resistivity. To further verify the distribution of PDSH within the ABS resin, EDS elemental analysis was performed on sections of ABS/PDSH-1091 containing 20 wt% PDSH as shown in Figure 8g–i, and the results showed that the different elements C, Cl, and O were uniformly distributed in the sections. The above results indicate that PDSH presents a uniform distribution in ABS, forming a continuous conductive network.

3.6 Mechanical characteristics

The tensile strength and notched impact strength of ABS/PDSH composites in relation to PDSH addition are shown in Figure 9a and b, respectively. The results showed that by increasing the addition of PDSH or decreasing the content of the ST component, the tensile strength and notched impact strength of the composites decrease to a certain extent. For example, the tensile strength of neat ABS was 46 MPa, and the notched impact strength was 20.3 kJ·m^{-2}. When the content of PDSH increased to 20 wt%, the tensile strength and notched impact strength decreased to 36 MPa and 14.7 kJ·m^{-2} for the ABS/PDSH-1091 composite and 33.4 MPa and 13.7 kJ·m^{-2} for the ABS/PMMD-1019 composite. The change in mechanical properties of the composite material is because there are more polar components in PDSH, which makes it easy to generate voids when blending with the matrix ABS resin. As the amount added increases, the number of internal voids also increases, and the creation of voids leads to a reduction in mechanical properties. Increasing the content of the ST component in

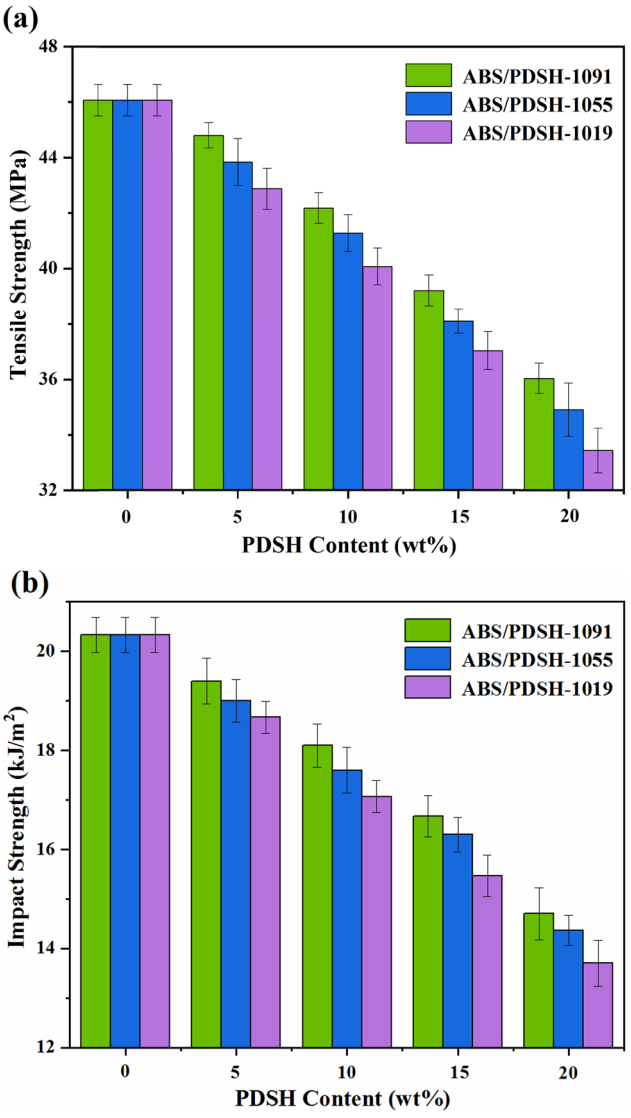

Figure 9: Influence of the PDSH content on the mechanical properties of ABS/PDSH composites: (a) tensile strength and (b) impact strength.

PDSH at the same additional amount can increase the compatibility of PDSH with the matrix resin and reduce the degradation of mechanical properties of the composite. The composite material can also maintain good mechanical properties under the appropriate additional amount.

4 Conclusion

In summary, a novel quaternary ammonium salt-based copolymer antistatic agent PDSH was synthesized and

characterized. The results showed that the PDSH effectively reduced the surface resistivity of ABS resins. The surface resistivity of ABS/PDSH composites decreased by about 10^6 times compared with pure ABS when the PDSH increased. Furthermore, the contact angle results indicated that the hydrophilicity of the composite was improved. PDSH was uniformly distributed within the ABS resin, and the composites could maintain good mechanical properties under the appropriate addition. In consideration of the properties described above, we conclude that the PDSH was an antistatic additive with good comprehensive properties and was suitable for ABS.

Funding information: This work was supported by the Guangdong University of Technology Industry Collaboration Program (Grant No. 607190080).

Author contributions: Chenming Zhang: writing – original draft, writing – review and editing, methodology, and formal analysis; Yihua Cui: writing – original draft, formal analysis, visualization, and project administration; Shiping Lin: resources and technical support; Jianwei Guo: writing – original draft, theoretical guidance, review, and editing of manuscripts.

Conflict of interest: Authors state no conflict of interest.

Data availability statement: All data generated or analyzed during this study are included in this published article.

References

(1) Olivera S, Muralidhara HB, Venkatesh K, Gopalakrishna K, Vivek CS. Plating on acrylonitrile–butadiene–styrene (ABS) plastic: a review. J Mater Sci. 2016;51(8):3657–74. doi: 10.1007/s10853-015-9668-7.

(2) Liu W, Wang H, Zou L, Cai S, Liu X, Liu J, et al. Synergistic effect of zeolite on the nitrogen-containing phosphinate salt-based acrylonitrile–butadiene–styrene flame-retardant composite. J Polym Res. 2021;29(1):1–9. doi: 10.1007/s10965-021-02811-8.

(3) Seo JS, Jeon HT, Han TH. Peeling mechanism of interlocked interface between etched acrylonitrile-butadiene-styrene and electroplated metal layer. Surf Interfaces. 2021;26:101337. doi: 10.1016/j.surfin.2021.101337.

(4) Han X, Wang G, He J, Guan J, He Y. Influence of temperature on the surface property of ABS resin in $KMnO_4$ etching solution. Surf Interface Anal. 2019;51(2):177–83. doi: 10.1002/sia.6560.

(5) Chen S, Xu C, Ma M, Shi Y, He H, Yuan K, et al. Application of solubility parameters in the preparation of PMMA with permanent antistatic, high toughness, and excellent optical properties. Polym Advan Technol. 2021;32(9):3750–8. doi: 10.1002/pat.5394.

(6) Wu W, Yang T, Zhang Y, Wang F, Nie Q, Ma Y, et al. Application of displacement-current-governed triboelectric nanogenerator in an electrostatic discharge protection system for the next-generation green tire. ACS Nano. 2019;13(7):8202–12. doi: 10.1021/acsnano.9b03427.

(7) Chen Y, Yao J, Xu M, Jiang Z, Zhang H. Electrically conductive and flame retardant graphene/brominated polystyrene/maleic anhydride grafted high density polyethylene nanocomposites with satisfactory mechanical properties. Chin J Polym Sci. 2019;37(5):509–17. doi: 10.1007/s10118-019-2220-5.

(8) Zhang J, Zuo J, Jiang Y, Ju A, Zhu D, Zhang J, et al. Synthesis and characterization of composite conductive powders prepared by Sb-SnO_2-coated coal gasification fine slag porous microbeads. Powder Technol. 2021;385:409–17. doi: 10.1016/j.powtec.2021.03.003.

(9) Chen S, Zhou B, Ma M, Shi Y, Wang X. Permanently antistatic and high transparent PMMA terpolymer: Compatilizer, antistatic agent, and the antistatic mechanism. Polym Advan Technol. 2018;29(6):1788–94. doi: 10.1002/pat.4285.

(10) Deschamps C, Simpson N, Dornbusch M. Antistatic properties of clearcoats by the use of special additives. J Coat Technol Res. 2019;17(3):693–710. doi: 10.1007/s11998-019-00283-6.

(11) Zheng A, Xu X, Xiao H, Li N, Guan Y, Li S. Antistatic modification of polypropylene by incorporating Tween/modified Tween. Appl Surf Sci. 2012;258(22):8861–6. doi: 10.1016/j.apsusc.2012.05.105.

(12) Tsurumaki A, Iwata T, Tokuda M, Minami H, Navarra MA, Ohno H. Polymerized ionic liquids as durable antistatic agents for polyether-based polyurethanes. Electrochim Acta. 2019;308:115–20. doi: 10.1016/j.electacta.2019.04.031.

(13) Yakovlev G, Pervushin G, Smirnova O, Begunova E, Saidova Z. The electrical conductivity of fluoroanhydrite compositions modified at the nanoscale level with carbon black. Environ Clim Technol. 2020;24(1):706–17. doi: 10.2478/rtuect-2020-0044.

(14) Wu J, Wang W, Chen X, Li N. Double percolation and segregated structures formed in polymer alloy with excellent electrical conductivity. Polym Compos. 2020;42(2):693–700. doi: 10.1002/pc.25858.

(15) Zhao S, Zheng M, Shen K. Ultrasound-assisted preparation of highly dispersion sulfonated graphene and its antistatic properties. J Text Inst. 2020;112(1):30–6. doi: 10.1080/00405000.2020.1746010.

(16) Omar SNI, Zainal Ariffin Z, Zakaria A, Safian MF, Halim MIA, Ramli R, et al. Electrically conductive fabric coated with polyaniline: physicochemical characterisation and antibacterial assessment. Emerg Mater. 2020;3(4):469–77. doi: 10.1007/s42247-019-00062-4.

(17) Zhuang Y, Tang X, Chang X, Cui L, Jiang B, Zhu B, et al. Self-assembly and antistatic property of poly(styrene sulfonic acid)-based graphene oxide liquid crystal compounds. Liq Cryst. 2021;1–11. doi: 10.1080/02678292.2021.2006810.

(18) Gill YQ, Ehsan H, Irfan MS, Saeed F, Shakoor A. Synergistic augmentation of polypropylene composites by hybrid morphology polyaniline particles for antistatic packaging applications. Mater Res Exp. 2020;7(1):015331. doi: 10.1088/2053-1591/ab61b5.

(19) Gurakin HK, Turan AC, Deligoz H. Synthesis of a novel polyester-ether copolymer and its derivatives as antistatic additives for thermoplastic films. Polym Test. 2020;81:14. doi: 10.1016/j.polymertesting.2019.106214.
(20) Li S, Wang J, Li Y, Wu G, Wang Y, Wang W, et al. Preparation and applications of the tertiary copolymer poly(ethylene glycol) methacrylate/methyl methacrylate/diethyl allylphosphonate. J Appl Polym Sci. 2016;133(44):44126–33. doi: 10.1002/app.44126.
(21) Bao L, Lei J, Wang J. Preparation and characterization of a novel antistatic poly(vinyl chloride)/quaternary ammonium based ion-conductive acrylate copolymer composites. J Electrost. 2013;71(6):987–93. doi: 10.1016/j.elstat.2013.09.001.
(22) Fu Y, Wang J, Zhao G, Wang Y, Chen S. Preparation and properties of poly(ether-ester-amide)/poly(acrylonitrile-*co*-butadiene-*co*-styrene) antistatic blends. J Appl Polym Sci. 2011;122(1):12–8. doi: 10.1002/app.33265.
(23) Wang S, Gonzales RR, Zhang P, Istirokhatun T, Takagi R, Motoyama A, et al. Surface charge control of poly(methyl methacrylate-*co*-dimethyl aminoethyl methacrylate)-based membrane for improved fouling resistance. Sep Purif Technol. 2021;279:119778–86. doi: 10.1016/j.seppur.2021.119778.
(24) Wei X, Liu M, Lu K, Wu H, Wu J. Friedel-Crafts alkylation modification and hydrophilic soft finishing of meta aramid. J Engineered Fibers Fabr. 2021;16:1–7. doi: 10.1177/1558925021999061.
(25) Sajjan AM, Premakshi HG, Kariduraganavar MY. Synthesis and characterization of GTMAC grafted chitosan membranes for the dehydration of low water content isopropanol by pervaporation. J Ind Eng Chem. 2015;25:151–61. doi: 10.1016/j.jiec.2014.10.027.
(26) Tsurumaki A, Tajima S, Iwata T, Scrosati B, Ohno H. Evaluation of ionic liquids as novel antistatic agents for polymethacrylates. Electrochim Acta. 2017;248:556–61. doi: 10.1016/j.electacta.2017.07.181.
(27) Kugimoto Y, Wakabayashi A, Dobashi T, Ohnishi O, Doi TK Kurokawa S. Preparation and characterization of composite coatings containing a quaternary ammonium salt as an antistatic agent. Prog Org Coat. 2016;92:80–4. doi: 10.1016/j.porgcoat.2015.11.013.
(28) Wang G, Xue B. Synthesis and characterization of poly(ether-block-amide) and application as permanent antistatic agent. J Appl Polym Sci. 2010;118(4):2248–53. doi: 10.1002/app.32357.
(29) Ji P, Jin J, Ji G, Wang C, Wang H. Investigation of the state and distribution of water in poly(ethylene terephthalate)/polyethylene glycol copolymers with various molecular weight of polyethylene glycol. Polym Eng Sci. 2015;55(10):2195–204. doi: 10.1002/pen.24104.